JOURNAL OF MATERIALS SCIENCE 26 (1991) 1375–1382

A study of corrosion fatigue behaviour of anodized and unanodized 2024-T3 aluminium alloy

G. C. TU, R. Y. HWANG*, I. T. CHEN
Department of Mechanical Engineering, National Chiao Tung University, Hsinchu, Taiwan

The corrosion fatigue (CF) behaviour, under constant deflection bending conditions with a pulsating tension stress form, of 2024-T3 aluminium alloy, unanodized and anodized to form a thick porous film, in 3.5% NaCl solution has been investigated. It was found that E_{corr} varies very little until specimen fracture under low frequency CF conditions, whereas E_{corr} drops rapidly when approaching the later fracturing stage of the CF process under high-frequency conditions for unanodized specimens. However, a slow drop in E_{corr} was detected from the commencement of the CF process, and lasted up to a much more rapid drop at a later fracturing stage for the anodized specimen. This behaviour presumably can be explained by the cracking of the anodic film and the theory of imperfect recovery of the surface film. It is suggested that the E_{corr} monitoring technique may be useful for determining the remnant CF life for existing structural parts of this alloy or other aluminium alloys regardless of whether or not they are anodized. Furthermore, the T3 temper provides a microstructure which may retard main-crack formation and penetration in the CF process of the anodized alloy, thus mitigating partly the negative effect of the readily crackable anodic film.

1. Introduction

The corrosion fatigue (CF) behaviour of anodized aluminium alloy is, in general, different from that of unanodized. Stickley and Lyst [1] found that a specimen anodized in sulphuric acid with a film thickness less than 25 μm exhibited no protection action to CF and with thicker films the situation became worse. They also found that a specimen anodized in chromic acid had a prolonged CF life under high-cycle CF conditions but little effect was detected under low-cycle CF conditions. Beital and Bowles [2] concluded that anodizing a 1100 aluminium to form a barrier-type film 30 to 150 nm thick had no effect on its CF life under low-cycle ($< 10^5$ cycle) conditions.

This study reports an electrochemical investigation of CF behaviour, under constant deflection bending conditions with a pulsating tension stress form, of anodized and unanodized 2024-T3 aluminium alloys in 3.5% NaCl solution. The porous film thicknesses were about 60 and 120 μm, simulating the thickness met under general hard anodizing conditions. It was the aim of this study to shed more light on the CF cracking mechanism of this particular alloy with and without a thick porous anodic film. The results show interesting findings which differ from those of ferrous alloy and 7xxx series aluminium alloy.

2. Experimental procedure

As-received 3 mm thick 2024-T3 aluminium alloy sheet (China Steel Corp.) was used as the raw material. The chemical composition and mechanical properties of the alloy sheet are shown in Tables I and II, respectively.

The shape and dimensions of the specimen for CF testing are shown in Fig. 1. In order to fracture the specimen in a limited area, the specimen is designed in such a way that the stress is nonuniformly distributed, i.e. both the straight sides of the normal equal-stressed triangle were curved inward as shown and the load is applied at the apex of the normal triangle. In this way the highest stress distribution, where eventual fractures occur, is located at the central dotted line within the cross-hatched area; this area covers 5 cm^2 and is also the anodized area.

All specimens were ground with emery paper to 1000 grit finish, cleaned ultrasonically in acetone and rinsed in distilled water. Except for the 5 cm^2 cross-hatched area, the whole specimen was coated with acid-resistant paint.

An SCR/RET d.c. power supply (0 to 150 V, 0 to 20 A) was used to anodize the alloy, taking advantage of the as-supplied pulsed SCR rectified power form (60 Hz) [3]. Both constant voltage and constant current mode of anodizing were adopted in the present work. Three types of specimen preparation were used throughout the work as shown in Table III. The criteria for choosing specimens B and C are to obtain a relatively thick and hard anodic film with relatively little cracking observable to the naked eye.

* *Present address*: Chung Shan Institute of Science and Technology, Lungtan, Taiwan.

0022–2461/91 $03.00 + .12

TABLE I Chemical composition of the test material (wt %)

Cu	Mg	Mn	Si	Cr	Al
3.8	1.2	0.5	0.2	0.06	bal.

TABLE II Mechanical properties of the test material

$\sigma_{0.2\%\ offset}$ ($kg\,mm^{-2}$)	σ_{UTS} ($kg\,mm^{-2}$)	Elongation (%)
29.7	44.2	12

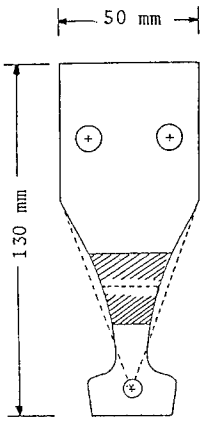

Figure 1 The shape and dimensions of the corrosion fatigue specimen.

TABLE III Specimen preparation conditions

Specimen	Preparation conditions
A	As-received 2024-T3 alloy sheet 3 mm thick, ground to 1000 finish
B	Specimen A anodized at 15 V in 20% H_2SO_4, 0 °C for 10 min to ~ 60 μm thick and 290 VPN hardness
C	Specimen A anodized at 20 V in 15% H_2SO_4, 0 to 4 °C for 10 min to ~ 120 μm thick and 240 VPN hardness

The arrangement of the apparatus for this investigation is schematically shown in Fig. 2. The cubic corrosion cell was made of acrylate and in which the specimen, graphite counter electrode, calomel reference electrode, cam shaft, and cam were immersed in the 3.5% NaCl solution. A PARC Model 173 potentiostat was employed to impose a constant potential upon the specimen and the resultant current/time variation recorded in a X–t recorder. A potentiodynamic method was used to determine the pitting potential (E_p) and protection potential (E_{pp}). The specimen was initially polarized to − 1000 mV (SCE) and then swept towards the noble direction at 0.2 mV sec^{-1}; the potential was reversed towards the active direction when the anodic current density increased suddenly, and continued until reaching the protection potential.

A pulsating tension strain, as shown in Fig. 3 was

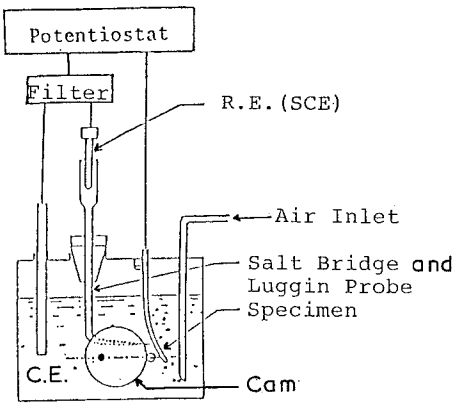

Figure 2 The arrangement of the testing apparatus.

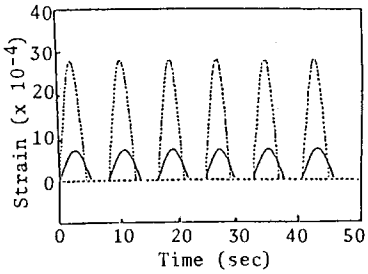

Figure 3 The pulsating tension strain form incurred on the specimen surface with cams of 1 and 5 mm deviation to the central line and a frequency of 8 c.p.m.

TABLE IV Relationship of applied stress and cam

Degree of cam deviation to centre line (mm)	Max. strain (Δe)	Max. stress ($\Delta\,kg\,mm^{-2}$)
3	$\Delta e_1 = 18.0 \times 10^{-4}$	12.4
5	$\Delta e_2 = 27.5 \times 10^{-4}$	19.0
7	$\Delta e_3 = 39.1 \times 10^{-4}$	27.0

applied to the specimen using a cam-controlled mechanism. The cams produce different deflections, which were measured by strain gauge, and hence different stress ($\sigma = E\varepsilon$). Young's modulus was experimentally determined to be $7.3 \times 10^3\ kg\,mm^{-2}$, and the relationship of the applied stress and cam is shown in Table IV.

3. Results and discussion

3.1. Relationship between E_{corr} and specimen type

The E_{corr} of 2024-T3 alloy is about − 720 mV (SCE). Specimen B assumes an E_{corr} of about − 713 mV (SCE), which is independent of film thickness. An E_{corr} of − 730 mV (SCE) is detected with the specimen formed at 1.25 A in 20% H_2SO_4 at 0 °C, which is also independent of film thickness. In summary, E_{corr} is mainly dependent upon the specimen preparation conditions, but is independent of film thickness. Theoretically, different anodizing conditions may give rise to barrier layers with different corrosion resistances, and hence different E_{corr} values.

3.2. Relationship between E_p, E_{pp} and film thickness

E_p and E_{pp} of 2024-T3 alloy are about -620 and -745 mV (SCE), respectively; this can be seen readily from Fig. 4 which shows the E/I relationship through a potentiodynamic scanning process. The E/I diagram of specimen B is shown in Fig. 5.

Comparing Figs 4 and 5, it is apparent that a much larger current occurs in the latter case after reversing the potential. Fig. 6 shows the appearance of specimen A after the potentiodynamic scanning process; it is clear that many small and shallow pits result. Fig. 7 shows the appearance of specimen B after the potentiodynamic scanning process; a much smaller number but larger pits are evident (Fig. 7a). Furthermore, from the cross-section of the specimen (Fig. 7b), the undermining of a relatively large area below each pitted hole is clearly illustrated. It is reasonable to assume that this undermining of a relatively large area is responsible for the much larger current detected in Fig. 5.

3.3. The variation of E_{corr} during the CF process

During the CF of 2024-T3 alloy, E_{corr} fluctuates slightly ($\pm$ 2 to 5 mV) corresponding to each cyclic stress, being in the anodic direction the stress-raising stage and in the cathodic direction during the stress-relieving stage.

Fig. 8 shows the variation of E_{corr} for specimen A at various cycles at Δe_3. It shows that at 8 c.p.m. E_{corr} although fluctuating ($\pm$ 2 to 5 mV) in each cycle, varies very little with cycle number; an enlarged display of the variation of E_{corr} within each cycle at 8 c.p.m. after $\sim$ 11 000 cycles is shown in Fig. 9a. At 20 c.p.m. a gradual drop of E_{corr} is detected at the later stage, and at 78 c.p.m. an earlier and more rapid drop of E_{corr} is apparent at the later stage. An enlarged display of the variation of E_{corr} within each cycle at 78 c.p.m. after $\sim$ 12 500 cycles is shown in Fig. 9b. Fig. 10 shows the effect of strain on the E_{corr}/time behaviour for specimen A. It is evident that higher strain results in an earlier and more rapid drop in E_{corr}.

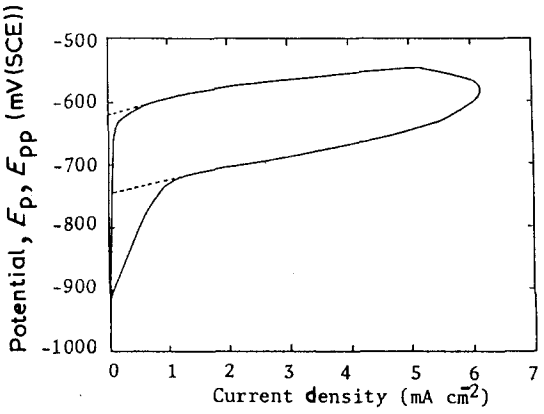

Figure 4 The E/I behaviour for potentiodynamic scanning of 2024-T3 alloy in 3.5% NaCl solution with E_p and E_{pp} adopted as indicated by the dotted line.

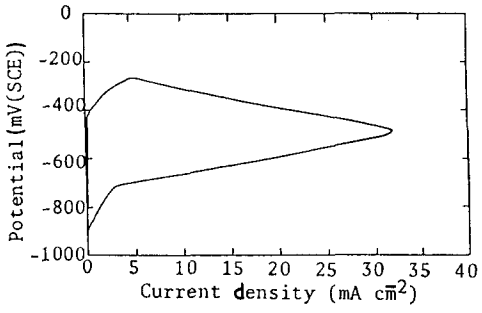

Figure 5 The E/I behaviour for potentiodynamic scanning of anodized 2024-T3 alloy (to 60 μm) in 3.5% NaCl solution.

Fig. 11 shows a similar effect of strain on the E_{corr}/time behaviour for specimen B as for specimen A (Fig. 10), except that apparently E_{corr} drops gradually from the very beginning of the CF process for specimen B, in contrast to the nearly constant E_{corr} maintained until later stages for specimen A. However, the later rapid E_{corr}-dropping behaviour when approaching fracture is the same for both specimens A and B.

Fig. 12 compares the E_{corr}/time behaviour between specimens A, B and C. It demonstrates clearly that E_{corr} of anodized specimens B and C drops at an earlier stage and hence a shorter life than that of unanodized specimen A is expected.

Endo and Komai [4] studied the CF of high carbon steel under similar cyclic stress wave forms, and found a small fluctuation ($\pm$ 0.2 to 0.5 mV) of E_{corr} within each strain cycle, and also as the CF process commences E_{corr} drops immediately and rapidly towards the active direction and then slows down, the rate gradually dropping until fracture as shown in Fig. 13 [4]. This behaviour of E_{corr} was explained by the E_{corr} variation within each cycle at different stages of the whole CF life [4]. Endo and Komai [4] also studied the CF process of high-strength aluminium alloy (7xxx) under certain stress wave forms and concluded that E_{corr} does not change with the number of stress cycles. The explanation for this is a perfect recovery in the cathodic direction, which also implies a perfect recovery of the activated surface during the zero stress period as shown in the wave forms A and B in Fig. 14 [4] within each cycle throughout the CF life.

The present results evidently show different CF behaviour for unanodized and anodized 2024-T3 alloy, from that of high-carbon steel and high-strength aluminium alloy (7xxx) [4]. For anodized 2024-T3 alloy, the present result differs from that of 7xxx alloy [4] in that under most conditions E_{corr} exhibits a rapid-dropping stage when approaching fracture; the only exception lies in the case of CF at 8 c.p.m. (Fig. 8) which shows little variation of E_{corr} until fracture; this behaviour is in accordance with Endo and Komai's result for 7xxx alloy. The results in Fig. 8 are presumably explicable as follows; at 8 c.p.m. the longer stress-relieving time allows a perfect recovery of the activated ruptured surface during the crack propagation period, this maintains a constant E_{corr} until fracture as can also be deduced from Fig. 9a; at 20 and 78 c.p.m. the shorter stress-relieving time eventually makes perfect film recovery more or less difficult, as is

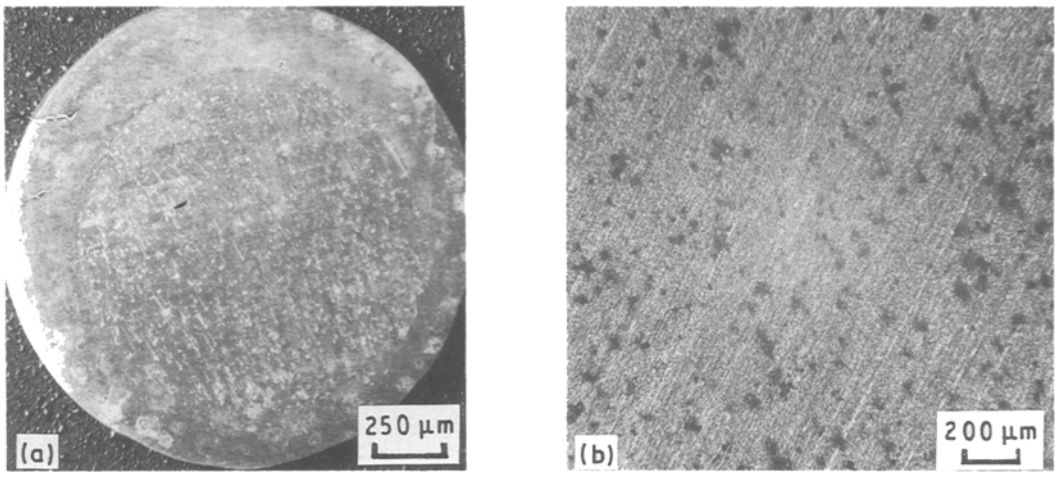

Figure 6 The surface appearance of specimen A after potentiodynamic scanning in 3.5% NaCl solution.

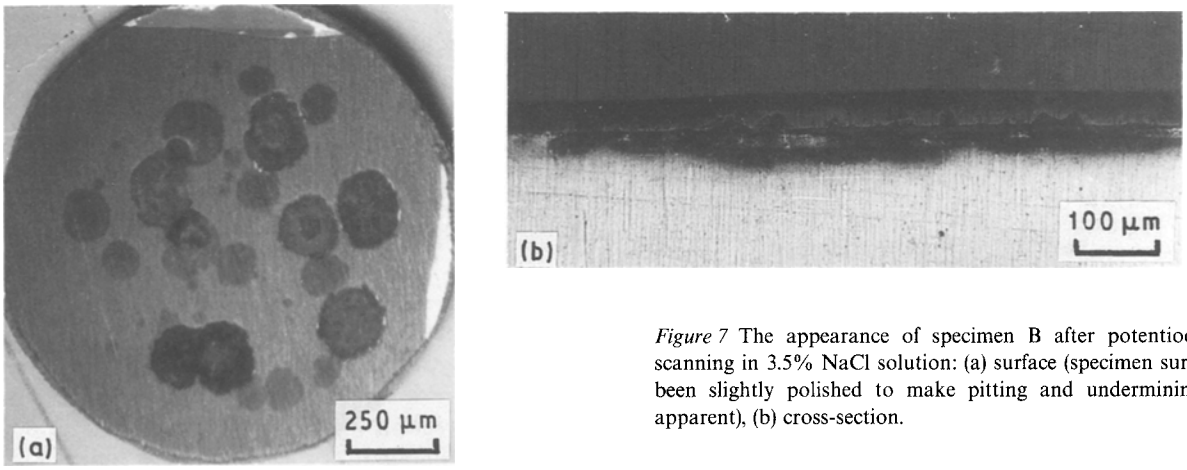

Figure 7 The appearance of specimen B after potentiodynamic scanning in 3.5% NaCl solution: (a) surface (specimen surface has been slightly polished to make pitting and undermining more apparent), (b) cross-section.

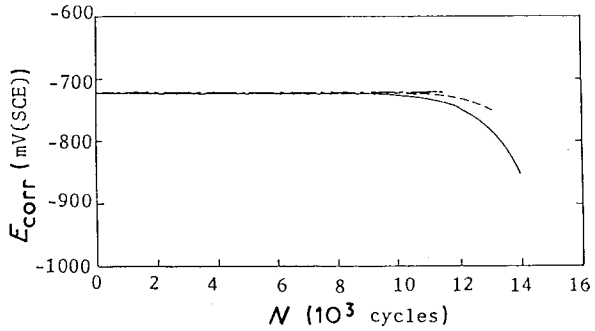

Figure 8 The E_{corr}/cycle behaviour at (—·—) 8 c.p.m., (——) 20 c.p.m., and (——) 78 c.p.m. for specimen A at Δe_3.

evident in Fig. 9b, which may accelerate crack propagation and provide an ever-increasing area under imperfect or unprotected status as CF continues, this causes a rapid drop of E_{corr} when fracture of the specimen is approached. Apparently, for unanodized 2024-T3 alloy, the strain magnitude can also be a factor in determining the E_{corr} variation in the whole CF process (Fig. 10).

Comparing Figs 10 and 11, it can be seen that E_{corr} of the anodized specimen drops immediately although very slowly once CF proceeds and that of the unanodized specimen remains nearly constant for most of its CF life; this could imply that the anodic film is probably cracked more or less at the very beginning of the CF process and that the cracks penetrate into the substrate, whereas the unanodized specimen takes a much longer time for cracks to be formed by corrosion of the naturally formed thin surfacial film and intrusion and extrusion mechanism; alternatively, this could imply that a perfect recovery of the surface film adjacent to crack tips could possibly be more difficult for the anodized specimen due to the presence of a thick porous film, which could retard the access of oxygen or make it difficult for refreshing of the solution to the newly cracked area near the crack tip. Probably both mechanisms operate consecutively.

For practical purposes, the present findings of the rapid drop in E_{corr} when approaching fracture can be employed as a means to determine the remnant CF life for critical structural parts made of this alloy and facilitate maintenance work. It is also envisaged that other aluminium alloys may also present similar behaviour to 2024-T3 alloy, provided they can be operated at appropriate frequency, cyclic stress wave form, electrolyte, etc.

Further comparison of the present work with that of Endo and Komai on high-carbon steel (as can be seen from Figs 10, 11 and 13), reveals that an imperfect recovery occurs until fracture for high-carbon steel

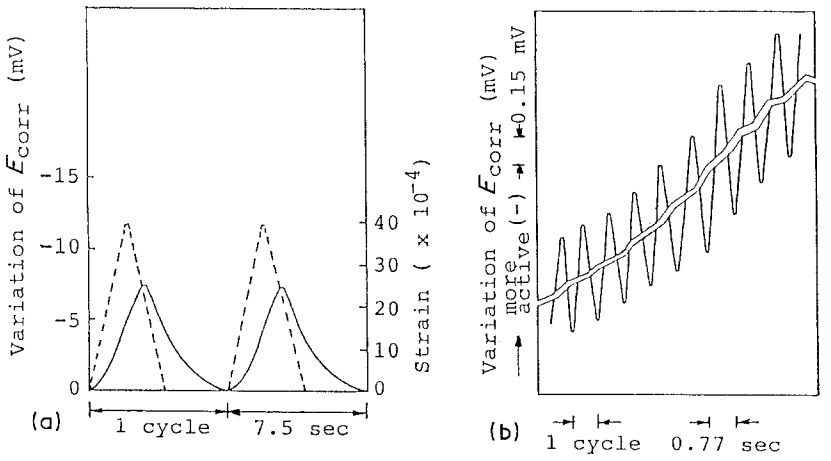

Figure 9 The variation of E_{corr} within each cycle at Δe_3 during CF process for specimen A: (a) at 8 c.p.m. after ~ 11 000 cycles, (b) at 78 c.p.m. after 12 500 cycles. (a) (– – –) Strain, (——) E_{corr}.

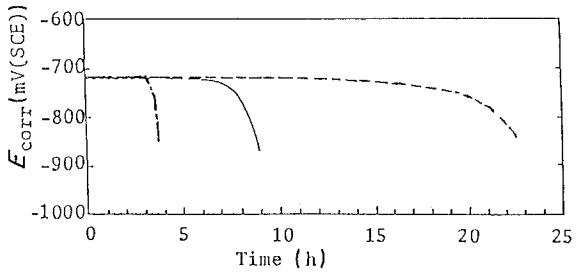

Figure 10 The E_{corr}/time behaviour at (– – –) e_1, (——) e_2, (—·—) e_3 for specimen A at 78 c.p.m.

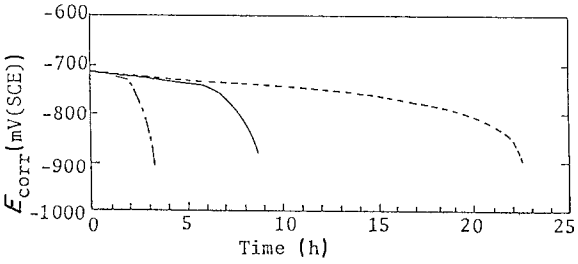

Figure 11 The E_{corr}/time behaviour at (– – –) e_1, (——) e_2, (—·—) e_3 for specimen B at 78 c.p.m.

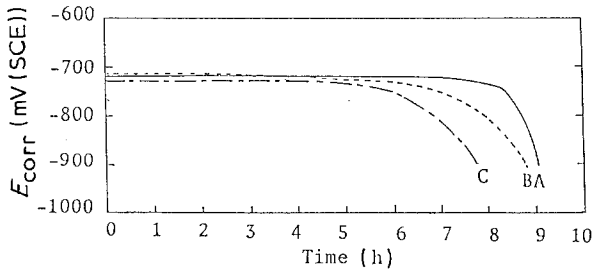

Figure 12 The E_{corr}/time behaviours for specimens A, B and C corrosion-fatigued at Δe_2 at 78 c.p.m.

(Fig. 13), whereas a larger extent of recovery is evident in Figs 10 and 11 for unanodized and anodized 2024-T3 alloy for most of their CF lives, except on reaching the stage approaching fracture. Obviously, the E_{corr} monitoring technique is essentially useless for determining the remnant CF life of structural parts made of high-carbon steel.

3.4. The variation of anodic current during the CF process

A constant potential of – 680 mV (SCE) which is anodic to the corrosion potential (E_{corr}) but cathodic to the pitting potential (E_p) of specimens A, B and C, is maintained on the specimen during the CF process, enabling monitoring of the anodic current variation with time. Fig. 15 shows anodic current/time behaviour for specimens A, B and C at Δe_3, and Fig. 16 shows that at Δe_2.

Both Figs 15 and 16 show that the anodic current of Specimen A rises to a much less extent than both specimens B and C from the commencement of stress application, then increases linearly and followed by a levelling-off period before increasing again at the stage prior to fracture; higher strain also results in higher current and more rapid current increasing rate in the early stage. The behaviour of specimen B is similar to that of specimen A, except that the former shows a current-drop period, which is shown more clearly in Fig. 16. For specimen C, the highest current among the three specimens was monitored throughout the CF life. The difference in the current magnitude at the initial rise perhaps suggests that films, either anodic or surfacial, are least readily crackable for specimen A and most readily for specimen C. Also, the difference in the current magnitude at the later levelling-off period indicates that the crack opening rate and/or the film recovery rate are in the sequence of C > B > A for the former and A > B > C for the latter. The reason for the drop in current for specimen B in the levelling-off period is not clear yet. It is also interesting to note that the CF lives for the three specimens increase as the total applied current (i.e. the integration of the area underneath each curve in Figs 15 and 16) decreases.

3.5. Corrosion fatigue life

Fig. 17 shows the CF lives at various strains for specimens A, B and C under open potential conditions. Under higher strain conditions (Δe_3), similar lives for the three specimens were detected; however, the scattering of lives become more apparent under lower strain conditions (Δe_1). It is probably the strain factor that dominates under higher strain conditions

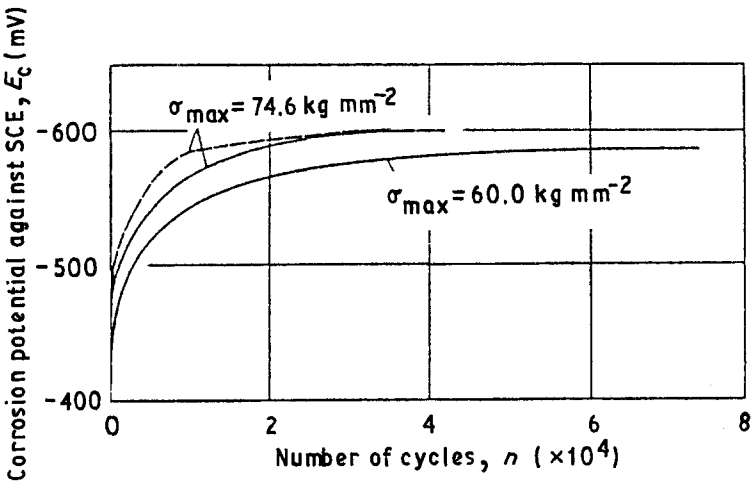

Figure 13 The variation of E_{corr} with number of cycles during the CF process for high-carbon steel [4]. (– – –) 2.44 sec, (——) 1.18 sec.

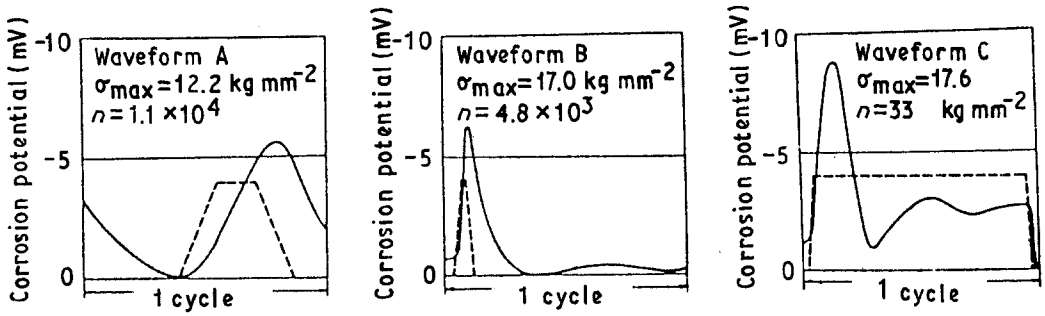

Figure 14 The variation of (——) E_{corr} and (– – –) stress during one cycle under various stress wave forms for 7xxx series aluminium alloy [4].

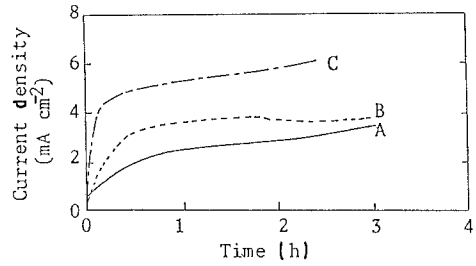

Figure 15 The current density/time behaviour for specimens A, B and C corrosion-fatigued at Δe_3 at 78 c.p.m. with an applied constant potential of – 680 mV (SCE).

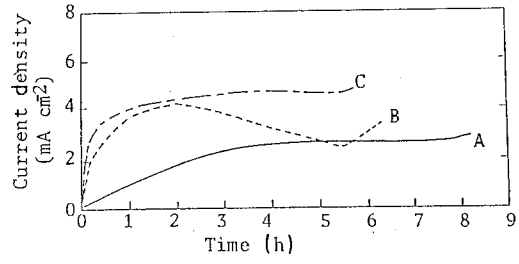

Figure 16 The current density/time behaviour for specimens A, B and C corrosion-fatigued at Δe_2, 78 c.p.m. with an applied constant potential of – 680 mV (SCE).

which facilitates an earlier main crack formation among the three specimens; whereas, under lower strain conditions, a longer initiation period is required for the main crack formation, during which time the corrosion factor could possibly play an important role, and manifests the different degree of corrosion

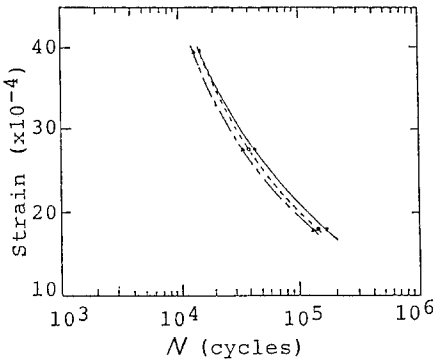

Figure 17 The strain/fatigue life curve for specimens A, B and C corrosion-fatigued at 78 c.p.m.

resistance among the three specimens in the wider scattering of the CF life.

Fig. 18 shows the CF lives at various strains for specimens A, B and C under conditions of constant potential of – 680 mV (SCE). This figure shows that the CF lives are generally shortened to a larger extent as the strain decreases, and also a wider scattering of the CF lives than that under open potential and lower strain condition can be readily sensed. The above findings strongly support the assumption that corrosion dominates the corrosion fatigue at lower strain.

3.6. Fracture of anodic film and growth of the main crack

Fig. 19 shows the cracks on the film surface for specimen B corrosion-fatigued at Δe_3 for 1000 cycles (the

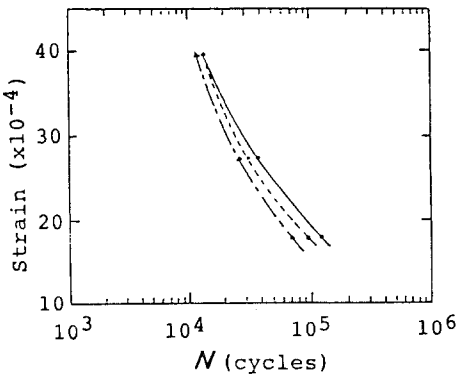

Figure 18 The strain/fatigue life curve for specimens (——) A, (– – –) B and (– · –) C corrosion-fatigued at 78 c.p.m. with an applied constant potential of – 680 mV (SCE).

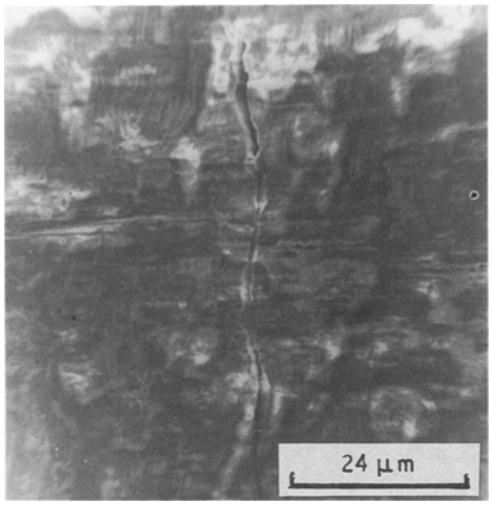

Figure 19 The surfacial crack appearance for specimen B after being corrosion-fatigued at Δe_3 for 1000 cycles.

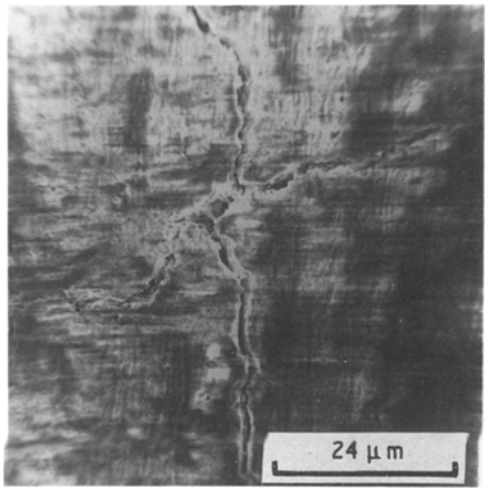

Figure 20 The surfacial crack appearance for specimen C after being corrosion-fatigued at Δe_3 for 200 cycles.

total life is about 15400 cycles) it is evident that cracking of anodic film occurs in the early stage of the CF process. Fig. 20 shows an even earlier cracking, after 200 cycles (the total life is about 13000 cycles) of anodic film for specimen C corrosion-fatigued at Δe_3.

Fig. 21 shows more clearly the cracking of the anodic film and the growth of the main crack for specimen B corrosion-fatigued at Δe_1. Fig. 21a and b show the cracking of the anodic film and the shallow penetration (about 0.18 mm) of this cracking into the substrate after 60000 cycles (the total life is 104400 cycles). It is interesting to find that extensive intergranular corrosion, perpendicular to the cracking direction, occurs due to the microstructure developed by the cold working in T3 treatment; this indicates that even though a film crack may be formed earlier in the CF process, it takes a much longer time for the film crack to develop into a precursor of a main crack. The reason is as follows; in one aspect, the elongated intergranular interface is presumably weaker to a certain extent than the grain, which would reduce the tensile triaxiality ahead of the crack tip, thus crack propagation will be retarded to a certain extent. In the second, the existence of the much weaker corroded intergranular interface would blunt the crack tip to a great extent and forms "crack arrester geometry" [5], which also makes it difficult for the crack to reinitiate in the adjacent layer, with the result that the toughness of the specimen is improved markedly. Fig. 21c and d show a yet later stage of propagation, after 100000 cycles which is approaching the fracture stage, of the main crack which penetrates 1.8 mm into the substrate; it is clear that little intergranular corrosion, as seen in Fig. 21a and b, occurs during propagation of the main crack and transgranular cracking is evident. It should be noted here that during the earlier CF process, many cracks are initiated and Fig. 21a and b show the typical deepest-penetrated crack observed. Until the later stage, many of the early-initiated cracks die out, and the typical deepest-penetrated crack can be readily selected as shown in Fig. 21c and d.

4. Conclusions

1. In comparison with an unanodized specimen anodized 2024-T3 alloy presents a nobler E_p but a similar E_{pp}, and its E_{corr} varies between – 710 and – 730 mV (SCE) depending upon the anodizing conditions.

2. During the CF process, monitoring the variation of E_{corr} helps to reveal the CF mechanism of unanodized and anodized alloys. It was found that E_{corr} varies very little until specimen fracture under low-frequency CF conditions, despite the fact that E_{corr} drops rapidly when approaching the later stage of the CF process prior to fracture under high-frequency conditions for unanodized specimens. However, a slow drop in E_{corr} was detected from the commencement of the CF process for anodized specimens and this lasted until a much more rapid drop at a later stage prior to fracture; this contrasted sharply with the nearly constant E_{corr} of the unanodized specimen which lasted for most of its CF life. This behaviour can be explained by the cracking of the anodic film and the theory of imperfect recovery of the surface film.

3. The technique of monitoring E_{corr} during the CF process is suggested to be useful for determining the remnant CF lives for existing structural parts of

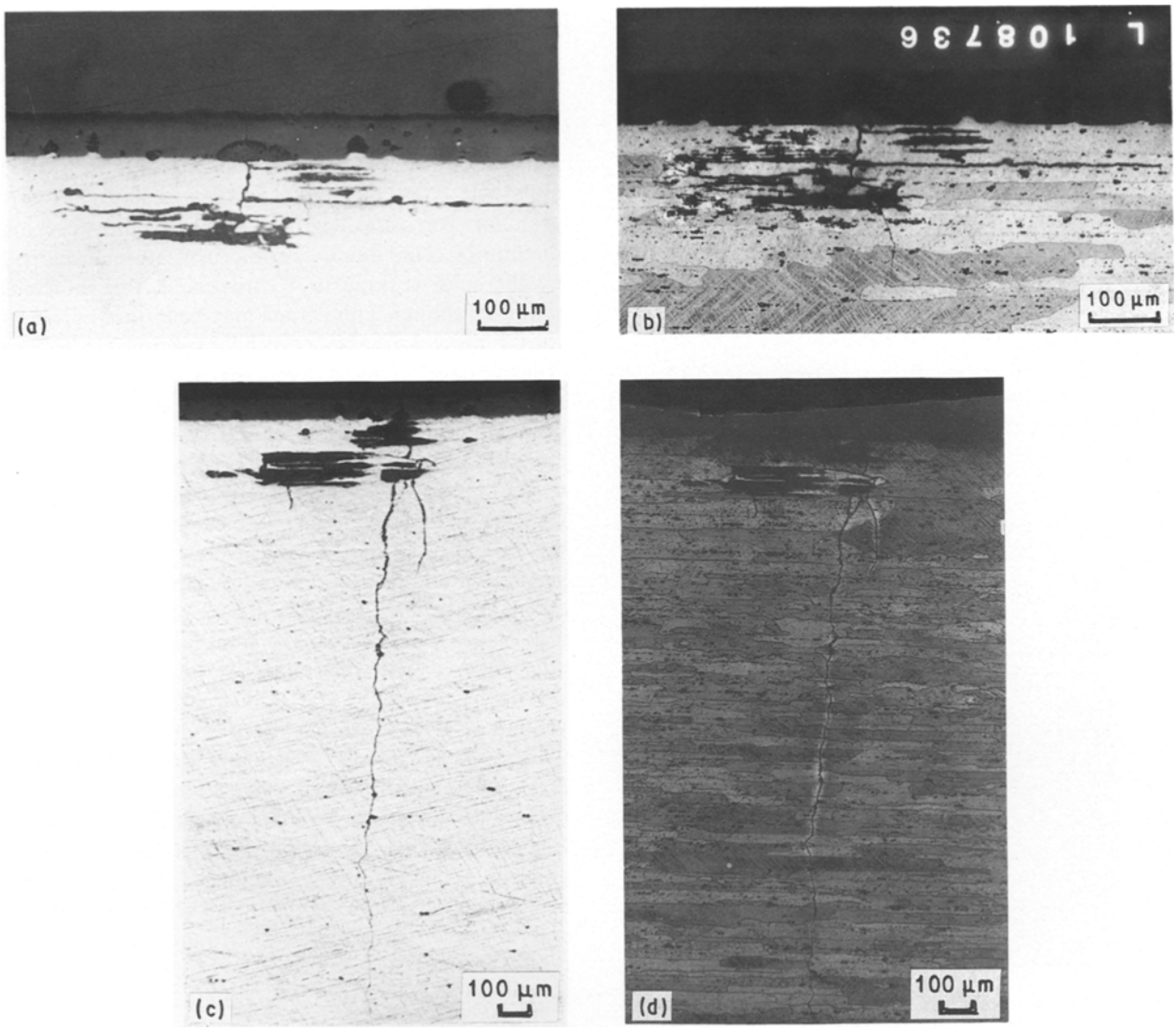

Figure 21 The cross-section appearance of specimen B after being corrosion-fatigued at Δe_1 for (a, b) 60 000 cycles, (c, d) 100 000 cycles (the total CF life is 104 400 cycles). (a, c) Before etching, (b, d) after etching.

2024-T3 alloy, or, perhaps, other aluminium alloys regardless of whether or not they are anodized.

4. The thick anodic films in the present study appear to be readily crackable, the readiness increasing as the cyclic strain and film thickness increase.

5. The T3 temper of the alloy provides an underfilm intergranular corrosion which retards main crack formation and penetration in the CF process of the anodized alloy. This mitigates partly the negative effect of the film for being readily crackable.

Acknowledgements

The authors thank the National Science Council of the Republic of China, for financial support of the project, and China Steel Corporation for supplying the raw material alloy sheet.

References

1. G. W. STICKLEY and J. O. LYST, *J. Mater.* **1** (1966) 19.
2. G. A. BEITAL and C. Q. BOWLES, *Met. Sci. J.* **5** (1971) 85.
3. G. C. TU and L. Y. HUANG, *Trans. Inst. Met. Fin.* **65** (1987) 60.
4. K. ENDO and K. KOMAI, "Corrosion Fatigue", edited by O. Devereux, A. J. McElivy and R. W. Staehle (National Association of Corrosion Engineers, Houston, USA, 1972) p. 437.
5. R. W. HERTZBERG, in "Deformation and Fracture Mechanics of Engineering Materials", 3rd Edn (Wiley, New York, 1989) p. 361.

Received 6 October
and accepted 1 December 1989